Modelling neuroanatomical variation due to age and sex during childhood and adolescence

Gareth Ball[1], Chris Adamson[1], Richard Beare[1] and Marc L. Seal[1,2,3]

1. Developmental Imaging, Murdoch Childrens Research Institute.
2. Department of Paediatrics, University of Melbourne
3. Data used in preparation of this article were obtained from the Pediatric Imaging, Neurocognition and Genetics Study (PING) database (http://ping.chd.ucsd.edu). As such, the investigators within PING contributed to the design and implementation of PING and/or provided data but did not participate in analysis or writing of this report. A complete listing of PING investigators can be found at https://ping-dataportal.ucsd.edu/sharing/Authors10222012.pdf.

Corresponding author:

Dr Gareth Ball
Developmental Imaging,
Murdoch Childrens Research Institute,
The Royal Children's Hospital,
Flemington Road
Parkville 3052
Melbourne, Australia

gareth.ball@mcri.edu.au

Abstract

Brain development is a dynamic process that follows a choreographed trajectory during childhood and adolescence with tissue-specific alterations that reflect complex and ongoing biological processes. Accurate identification and modelling of these anatomical processes *in vivo* with MRI may provide clinically useful imaging markers of individual variability in development. In this study, we build a model of age- and sex-related anatomical variation using multimodal imaging measures and manifold learning.

Using publicly-available data from two large, independent developmental cohorts (n=768 and 862), we apply a multimodal machine learning approach combining measures of tissue volume, cortical area and cortical thickness into a low-dimensional data representation.

We find that neuroanatomical variation due to age and sex can be captured by two orthogonal patterns of brain development and we use this model to predict age with a mean error of 1.6-2 years and sex with an accuracy of 80-84%.

We present a framework for modelling anatomical development during childhood using low-dimensional data representations. This model accurately predicts age and sex based on image-derived markers of cerebral morphology and generalises well to independent populations.

Keywords

brain development; magnetic resonance imaging; machine learning; cognition; manifold embedding

Introduction

Brain development is a dynamic process that follows a choreographed trajectory during childhood and adolescence. During this formative period the brain undergoes profound change: brain volume increases rapidly between the ages of 3 and 18 (Dekaban 1978); while myelination processes that begin *in utero* continue through to the second decade of life (Yakovlev and Lecours 1967), and cortical pruning leads to significant reductions in synaptic density during early adolescence (Huttenlocher 1979).

Magnetic resonance imaging (MRI) provides the opportunity to study brain development and track developmental processes *in vivo*. Analyses of structural MRI data have found that grey and white matter volumes follow different trajectories during adolescence. Cortical grey matter volume is greatest in childhood, then gradually decreases during adolescence (Tamnes et al. 2013; Mills et al. 2016), whereas white matter volume increases throughout childhood and adolescence (Lebel and Beaulieu 2011; Aubert-Broche et al. 2013). In contrast, measures of cortical thickness show progressive thinning from mid-childhood through to the early 20s (Raznahan et al. 2011) whereas cortical surface area appears to follow a cubic trajectory, peaking in late childhood before declining through adolescence (Wierenga et al. 2014). Beyond these global measures, Gogtay et al. observed significant regional variation in cortical development, with maturation in higher-order association cortices delayed compared to lower-order somatosensory and visual cortices (Gogtay et al. 2004). Similarly, Fjell et al. found that areal expansion in several cortical regions was greater than that of the average increase across the whole cortex; these included the anterior cingulate cortex, frontal cortex and insula (Fjell et al. 2015). Regional measures of cortical volume also show a differential effect of age, with changes in some regions (e.g.: medial parietal cortex) most apparent at younger ages, compared to others where the rate of change was greatest later in development (e.g.: the anterior temporal lobe) (Tamnes et al. 2013). Sex also likely plays a role in cerebral development. Sexual dimorphism has been observed in developmental studies of cortical thickness (Sowell et al. 2007) and sex-by-age interactions have been reported in frontal cortical surface area in adolescence (Koolschijn and Crone 2013). Conversely, other studies suggest that while cerebral developmental trajectories do not appear to differ significantly between sexes (Aubert-Broche et al. 2013) cortical volumes reach a peak later in males than in females, the timing of which may coincide with pubertal onset (Giedd et al. 1999; Lenroot et al. 2007).

Taken together, these studies present a consensus view of typical cerebral development. However, longitudinal studies of healthy populations have shown that individual development can deviate significantly from these canonical trajectories (Mills and Tamnes 2014). This suggests the presence of possible interactive effects of genes and environmental influences on brain development (Lenroot and Giedd 2008; Giedd et al. 2010; Richmond et al. 2016) and highlights the need to create models of typical growth and development of the brain that can be applied on an individual level. Establishing developmental trajectories for typical cerebral development is vital to our understanding of maturational brain change and may provide a more accurate understanding of relationships between brain maturation and behavioural phenotypes during development.

Recently, studies have shown that it is possible to use MRI to accurately predict an individual's age (Dosenbach et al. 2010; Franke et al. 2010; Brown et al. 2012). These methods involve the use of modern machine-learning techniques to extract informative morphological features to act as markers of cerebral maturation in a predictive model. Using such models, the difference between chronological age and age predicted from imaging has been framed as an index of accelerated or delayed development or aging, depending on the direction of the discrepancy (Franke et al. 2012; Cole et al. 2015; Löwe et al. 2016). For example, Franke et al. used a nonlinear, multivariate kernel regression model to predict age in a cohort of children and adolescents based on maps of grey matter volume (Franke et al. 2012). They were able to predict age accurately across the full age-range. Moreover, predicted brain age was found to be significantly lower in a small clinical population of preterm-born adolescents, suggesting a developmental delay in brain maturation (Franke et al. 2012). Recently, Erus et al. reported that a significant increase in predicted brain age compared to chronological age in childhood (predicted by a multi-modal MRI assessment) was indicative of precocious cognitive development (and *vice versa*), suggesting that complex cognitive phenotypes could be captured as variation along a single dimension of brain development (Erus et al. 2015).

In this study, we aim to build upon these studies by constructing a model of typical brain development during childhood and adolescence using manifold learning, exploiting a rich data source of MRI acquired in a large-scale developmental cohort (Jernigan et al. 2016). Manifold learning refers to a suite of dimension reduction techniques based on the intuition that high-dimensional datasets (such as MRI)

reside on an embedded low-dimensional, and possibly non-linear, manifold or subspace. As such it represents a natural setting for this problem. The aim is to learn a mapping between the high- and low-dimensional data representations while preserving certain statistical properties (e.g.: variance) of the original data. This form of dimension reduction allows for an easier and more intuitive interpretation of important model features while retaining the underlying nonlinear relationships present between individual datapoints in the original dataset.

We hypothesise that typical neuroanatomical variation due to age and sex during development can be accurately represented as a low-dimensional process. To test this theory, we use a multimodal approach, combining measures of tissue volume, cortical area and cortical thickness to build a model that predicts age and sex with high accuracy and generalises well to other developmental populations. We also test the hypothesis that deviation from this model is associated with cognitive performance in two large population-based cohorts.

Methods

Imaging data

To model typical neurodevelopment, 3 Tesla, T1-weighted MRI data were obtained from the PING Study (Jernigan et al. 2016). In total, n=773 images acquired from typically-developing (TD) children aged 3 to 21 years were available to download from NITRC (https://www.nitrc.org). After visual quality control assessment, n=768 participants were included in the study (mean age=12.3y; range: 3.2–21.0y; 404 male). Site-specific demographic data are shown in Table S1.

T1 images were acquired using standardized high-resolution 3D RF-spoiled gradient echo sequence with prospective motion correction (PROMO) at 9 different sites, with pulse sequences optimized for equivalence in contrast properties across scanner manufacturers (GE, Siemens, and Phillips) and models (Jernigan et al. 2016). Written parental informed consent was obtained for all PING subjects below the age of 18 and directly from all participants aged 18 years or older.

In addition to imaging data, participants undertook comprehensive behavioral and cognitive assessments (NIH Toolbox Cognition Battery, NTCB; (Akshoomoff et al. 2014) and provided a saliva sample for genome-wide genotyping. The NTCB comprises seven tests (Flanker, Picture Sequence, List Sorting, Picture Vocabulary, Reading, Dimensional Change Card Sorting, Pattern Comparison) that measure abilities across six major cognitive domains, including cognitive flexibility, inhibitory control, and working memory (Akshoomoff et al. 2014).

For model validation, a comparative neurodevelopmental population was obtained from the ABIDE and ABIDE-II datasets (Di Martino et al. 2014, 2017). These datasets represent a consortium effort to aggregate MRI datasets from individuals with autism spectrum disorder and age-matched typically-developing controls. For both studies, 3 Tesla, T1-weighted MRI were acquired from 17 sites; images and acquisition details are available at http://fcon_1000.projects.nitrc.org/indi/abide. All participating sites received local Institutional Review Board approval for acquisition of the contributed data. In addition to imaging data, phenotypic information including age, sex, IQ and diagnostic information were recorded and made available (Di Martino et al. 2014, 2017)

T1 images from typically-developing participants aged 21y and under in both ABIDE and ABIDE-II were downloaded and visually assessed for quality. In total, n=424 (346 male; mean age=13.69y) and n=439 (297 male; mean age=11.50y) participants were included from 17 and 15 sites in ABIDE and ABIDE-II, respectively. Site-specific demographic data are shown in Table S2.

Image processing

For all subjects, vertex-wise maps of cortical thickness and cortical area were constructed from T1 MRI with FreeSurfer 5.3 (http://surfer.nmr.mgh.harvard.edu). Briefly, this process includes removal of non-brain tissue, transformation to Talairach space, intensity normalisation, tissue segmentation and tessellation of the gray matter/white matter boundary followed by automated topology correction. Cortical geometry was matched across individual surfaces using spherical registration (Dale et al. 1999; Fischl et al. 1999, 2002; Fischl and Dale 2000).

In addition, whole-brain tissue volume maps were estimated using deformation-based morphometry (Ashburner et al. 1998; Rueckert et al. 2003). Each participant's T1 image was intensity normalised,

corrected for bias field inhomogeneities and aligned to MNI 152 space using diffeomorphic nonlinear registration (ANTs; (Avants et al. 2008; Tustison et al. 2010). Voxel-wise maps of volume change induced by the transformation were characterised by the determinant of the Jacobian operator, referred to here as the Jacobian map.

Prior to analysis, both tissue volume maps and cortical thickness and area maps were smoothed with a Guassian kernel of 10 FWHM.

Manifold learning

Neighbourhood preserving embedding (NPE) is a linear approximation to locally linear embedding (LLE; Roweis and Saul 2000) that seeks to find a transformation, P, to map a high-dimensional $n \times D$ dataset $X = \{X_1, X_2, \cdots, X_n\}$ into a low-dimensional $n \times d$ subspace $Y = \{Y_1, Y_2, \cdots, Y_n\}$ where $d \ll D$ and $Y = P^T X$ (He et al. 2005). Like LLE, and in contrast to other linear subspace methods (e.g.: PCA), NPE aims to preserve the local neighbourhood structure of the data. The process is illustrated in Fig 1A. For a given data point X_i, an adjacency matrix is first constructed, placing an edge between X_i and X_j only if X_j belongs to the set of k nearest neighbours of X_i. Following this, a set of weights, W, is calculated that approximately reconstruct X_i from its neighbours and a linear projection, P, sought to optimally preserve this neighbourhood structure in the low-dimensional space, Y (He et al. 2005). NPE confers additional benefits over LLE, in that the solution generalises to new datapoints allowing unseen data to be projected onto the manifold without re-calculating the embedding.

Local neighbourhoods are typically defined based on the Euclidean distance between samples in the high-dimensional space, however it is possible to introduce other constraints in order to conduct NPE in a supervised setting (Fig. 1B; He et al. 2005; Zeng and Luo 2007). For example, restricting local neighbourhoods to only include subjects from the same class to enhance group separation, or weighting similarities based on some other subject-specific attributes of interest (e.g.: age).

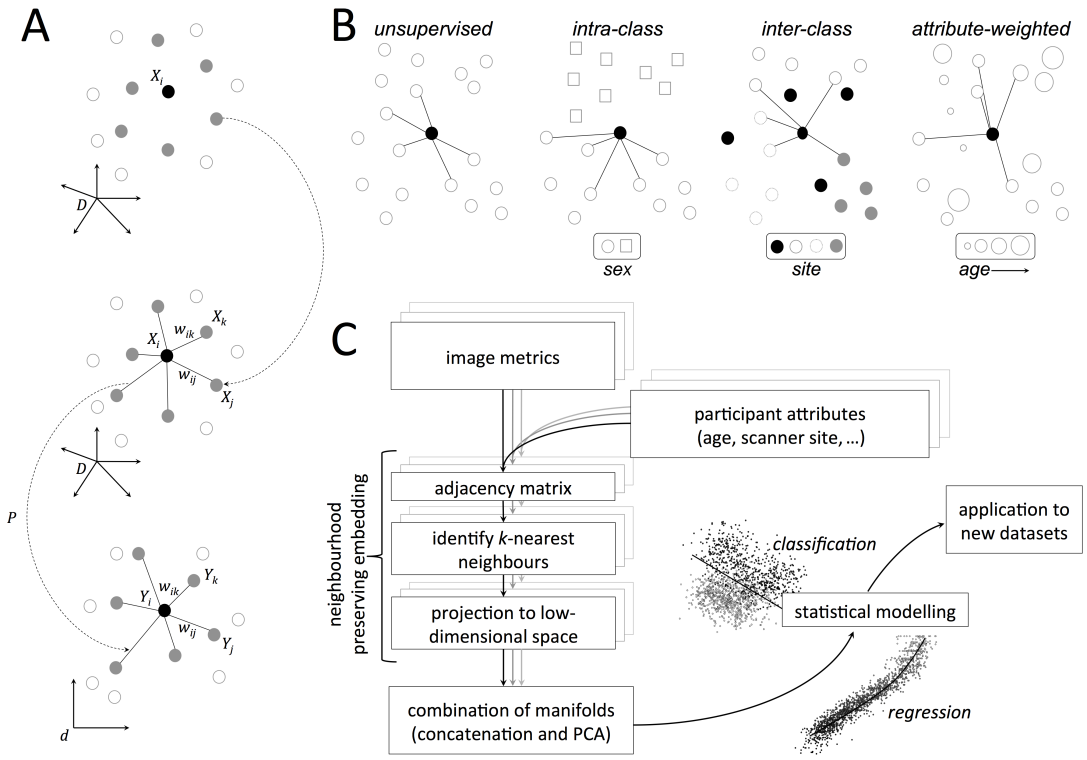

Figure 1: Neighbourhood preserving embedding and image analysis pipeline. A. For a given datapoint, X_i, nearest neighbours are selected and weights assigned that approximately reconstruct X_i. A projection, P, is then sought to transform the data into a low-dimensional space while preserving the neighbourhood structure. B. Possible supervision strategies for neighbourhood construction. In an unsupervised setting, neighbours are selected based on image similarity alone, alternatively, neighbours can be selected from within- or between-classes in order to maximise/minimise group differences in the manifold structure. Similarly, neighbours can be selected based on the weighted combination of image similarity and that of another subject-specific attribute (e.g.: age). C. Analysis pipeline for NPE analysis. For each image metric, NPE is used for subspace projection, before the embedded data are combined and passed on for statistical modelling.

The analysis pipeline used in this study is shown in Fig. 1C. For each image metric (tissue volume, cortical thickness, cortical area), data were first projected to an orthogonal subspace via singular value decomposition (SVD). Rank was automatically estimated according to (Minka 2001). NPE was then performed using $k = 10$ neighbours, projecting data to $d = 15$ dimensions. In order to maximally preserve age- and sex-related variation in the embedded data, we incorporated participant attributes into the construction of the adjacency matrices. Nearest neighbours were selected based on the product of two adjacency matrices, A and a, where the $(i,j)^{th}$ element of each matrix represents the (normalised) similarity between images, A, and age, a, of subjects i and j, respectively and $A_{i,j} = 0$, if $S_i \neq S_j$, where S indicates the sex of the participant. In order to reduce potential bias in image similarities due to site effects, we also introduced an additional constraint: $A_{i,j} = 0$, if $s_i = s_j$, where s indicates the site/scanner of image acquisition, although this had little effect on the final embedding.

This resulted in three sets of coordinates, Y_v, Y_t, and Y_a, representing the low-dimensional embedding of tissue volume, v, cortical thickness, t, and area, a, data. Due to likely overlap in the description of imaging data in the coordinate sets, we performed a final dimension reduction on the concatenated coordinate data, $Y_c = (Y_v, Y_t, Y_a)$ using PCA (Aljabar et al. 2011). This produced a final low-dimensional representation of the combined, multimodal image data for statistical analysis.

Code to perform NPE is available at: http://www.cad.zju.edu.cn/home/dengcai/Data/code/NPE.m

Statistical analysis

Internal validity of the learned manifold was assessed using 10-fold cross-validation. We used 90% of the PING participants as a training set, calculating the manifold embedding coordinates for each imaging modality and combining them into a single representation. To predict age, we fitted a polynomial model to the first joint embedding coordinate. To predict sex, the second coordinate was sent to a linear discriminant classifier. Image data from the remaining 10%, the test set, were then projected onto the joint manifold and the fitted models used to predict age and sex. Mean absolute error in age estimation (MAE) and correlation between true age and predicted age are reported, alongside classification accuracies for sex. This process was repeated for each fold, reconstructing the manifold each time, such that all PING participants were part of the test set exactly once.

External validity was assessed by projecting the combined ABIDE and ABIDE-II datasets onto a manifold constructed from the full PING dataset and predicting age and sex.

To determine if errors in image-derived age estimation correlated with cognitive performance, we performed a further set of analyses using available cognitive data. Of the PING dataset, n=617 had complete records for NTCB score, family socioeconomic status (household income and parental education), and genetic ancestry (Libiger and Schork 2012; Jernigan et al. 2016). NTCB scores were corrected for age, sex, socioeconomic status and GAF (Akshoomoff et al. 2014) and linear regression used to determine associations between age estimation error (based on cross-validated age predictions) and corrected cognitive scores.

For validation, in the ABIDE and ABIDE-II datasets, full scale IQ (FSIQ) was available for n=802 typically-developing participants (out of 863 combined across both studies). Using the same 10-fold cross-validation procedure outlined above, we derived age predictions for each participant and performed linear regression between age estimation error and FSIQ.

All statistical analysis was performed in Matlab R2105b (Natick, MA).

Results

Figure 2 shows manifold structure visualised as the first two embedding coordinates for tissue volume (Fig 2A), cortical area (Fig 2B) and cortical thickness (Fig 2C) calculated in the PING cohort. The images show the (standardised) weight of the embedding vectors used to project new data to the manifold.

For all three modalities, age is correlated with the first embedding coordinate, indicated by the gradation of colour along the first axis of the scatter plots Increasing age (a positive embedding coordinate) is associated with relatively increased tissue volume in the brain stem, and ascending white matter tracts subjacent to the primary motor cortex (positive image weights), with relative decreases in medial frontal and parietal cortices (negative image weights, Fig 2A). In the cortex, age is associated

with increasing surface area in the insula (Fig 2B) and reduced thickness across the frontal and parietal lobes, with increased thickness evident in the primary motor cortex and anterior temporal lobe (Fig 2C).

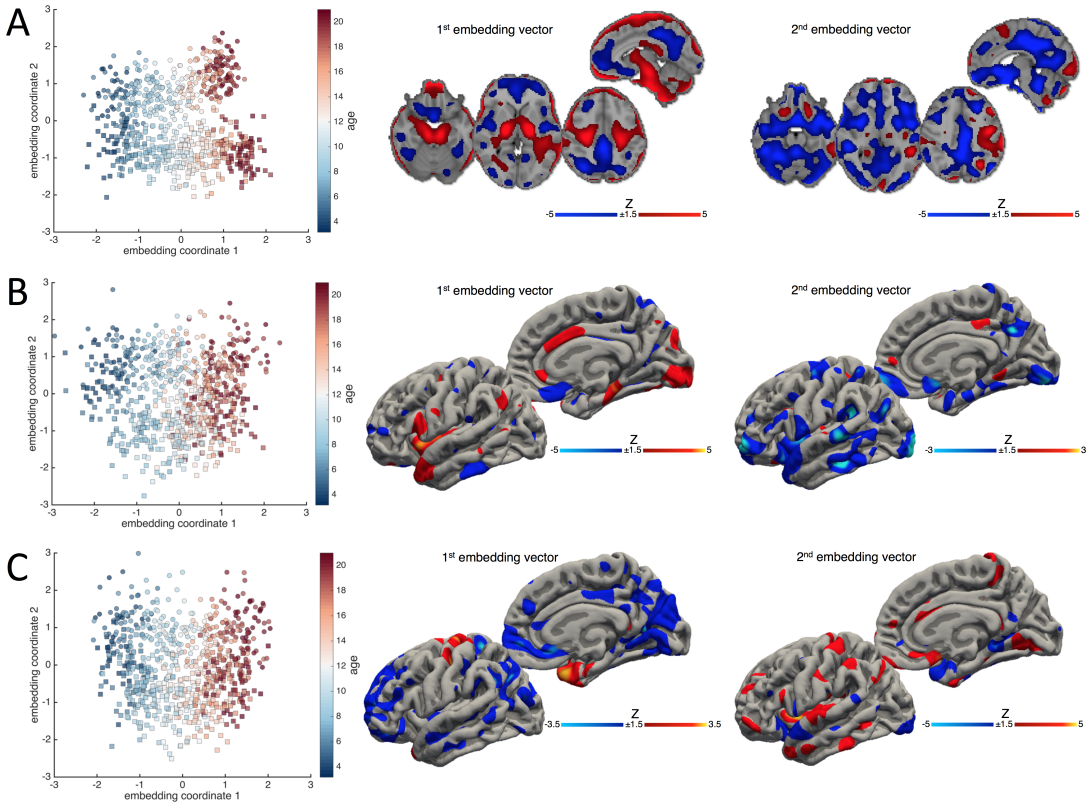

Figure 2: Manifold structure for tissue volume, cortical area and cortical thickness. Manifold structure is visualised for tissue volume (A), cortical area (B) and cortical thickness (C). For each image metric, the first two embedding coordinates are plotted against each other. Each point represents a subject; the colourbar indicates age and markers denote sex (square: male; circle: female). Images show the embedding vectors for the first and second coordinates, i.e.: the model coefficients each voxel required to transform data into the embedded subspace. Maps are Z-scored for comparison (colourbar).

Separation along the second dimension between sexes (squares and circles, Fig 2) appeared most apparent in tissue volume, with females demonstrating relatively reduced tissue volumes in medial parietal, insular, primary visual and medial temporal regions. Separation along the second dimension was also associated with decreased surface area in lateral temporal and orbitofrontal cortices, and increased thickness in the insula.

Figure 3A shows the joint manifold structure after combining all three image metrics. Anatomical variation due to age and sex are clearly captured along the first and second coordinates. Using 10-fold cross-validation, we predicted age with an MAE of 1.61 years (correlation between chronological and predicted age=0.915) by fitting a polynomial model to the first embedding coordinate of the joint manifold (Fig 3B). By applying a linear discriminant classifier to the second coordinate, we predicted sex with an accuracy of 83.6% (Fig 3B, left).

To determine if model accuracy varied with age, we partitioned our data into 10 approximately equal-sized bins and calculated MAE and classification accuracy within each bin (Table 1). Age prediction error ranged from a minimum of 1.15y at around 7 years of age, to a maximum of 2.87y in the oldest participants (mean age=20.3y). In contrast, classification accuracy ranged from 69% to 91%, with discrimination lowest in the youngest participants (mean age = 4.5y) and highest at around 16 years.

To demonstrate external validity of this approach, we repeated this analysis using a joint manifold constructed from the full PING dataset to predict age and sex in the ABIDE and ABIDE-II cohorts (Fig 4). We predicted age in ABIDE with an MAE of 1.83 years (correlation: 0.80), and sex with an accuracy of 78.1%. We achieved similar results in ABIDE-II (MAE=1.81, correlation: 0.76; accuracy=81.1).

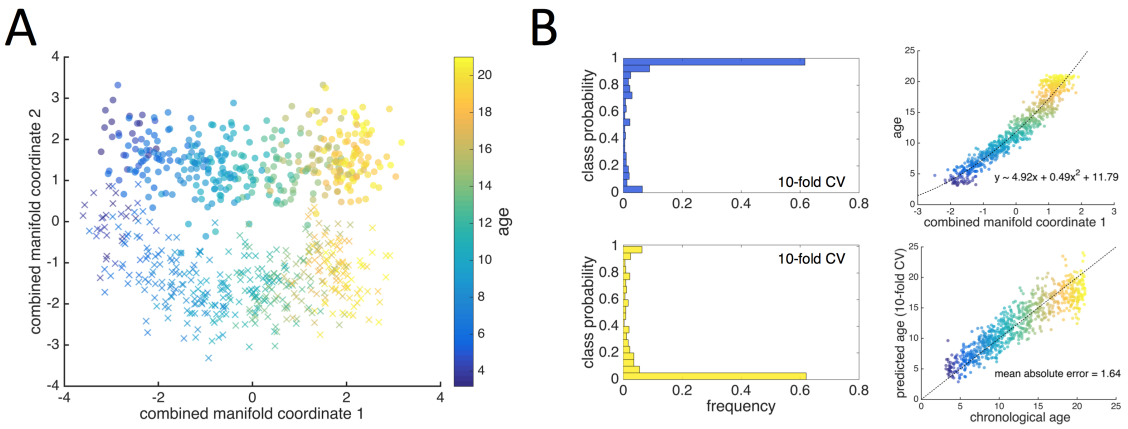

Figure 3: Age and sex prediction with manifold embedding. A. The first two coordinates of the joint manifold are shown, each point represents a subject; the colourbar indicates age and markers denote sex (cross: male; circle: female). B. Using 10-fold cross-validation, age and sex were predicted using on the first two embedding coordinates. Predicted class probabilities are shown for males (blue histogram) and females (yellow). To predict age, a polynomial model was fit to the first coordinate (top right); predicted age is shown plotted against chronological age (bottom right). Colourbar shown as in A.

Prediction accuracies in the PING cohort were robust to altering the number of neighbours, k, used in manifold construction (k=5: classification accuracy=83.5%, MAE=1.61; k=20: accuracy=83.6; MAE=1.62; k=50, accuracy=83.1, MAE=1.76). Performing supervised NPE without the additional constraint ensuring that nearest neighbours were selected from within the same sex did not significantly alter age prediction using the first manifold coordinate (MAE=1.59; correlation 0.91). Similarly, our model was robust to site variation as performing NPE without the additional site constraint did not affect the prediction accuracies (MAE=1.61y, accuracy=83.6%) and there was no significant association between acquisition site and absolute age estimation error (ANOVA: $F_{6,761}$ = 1.79, p=0.10). Performing the analysis using tissue volume maps corrected for total head size (by ignoring the affine scaling component in the calculation of the Jacobian map) did not alter our results (MAE=1.67, accuracy=82.8%).

Table 1: Age and sex prediction accuracy at different ages

Bin	n	mean age	MAE	male (%)	accuracy
1	75	4.48	1.51	38 (50.1)	69.33
2	79	7.31	1.15	44 (55.7)	84.81
3	71	8.96	1.26	38 (53.5)	83.10
4	79	9.63	1.25	35 (44.3)	83.54
5	77	11.72	1.53	43 (55.8)	84.42
6	80	12.89	1.68	52 (65.0)	86.25
7	77	14.52	1.52	47 (61.0)	83.12
8	76	16.15	1.64	36 (47.4)	90.79
9	74	17.63	1.88	34 (46.0)	81.08
10	80	20.29	2.87	38 (47.5)	88.75

To assess the individual contribution of each set of image metrics, we also performed the analysis using only tissue volume, cortical thickness or cortical area data. We found that the joint manifold combining all three metrics outperformed single metric models for both age and sex prediction (tissue volume only: MAE=1.78, accuracy=77.3%; area: MAE=2.99, accuracy=72.8%; thickness: MAE=1.96, accuracy=67.7%).

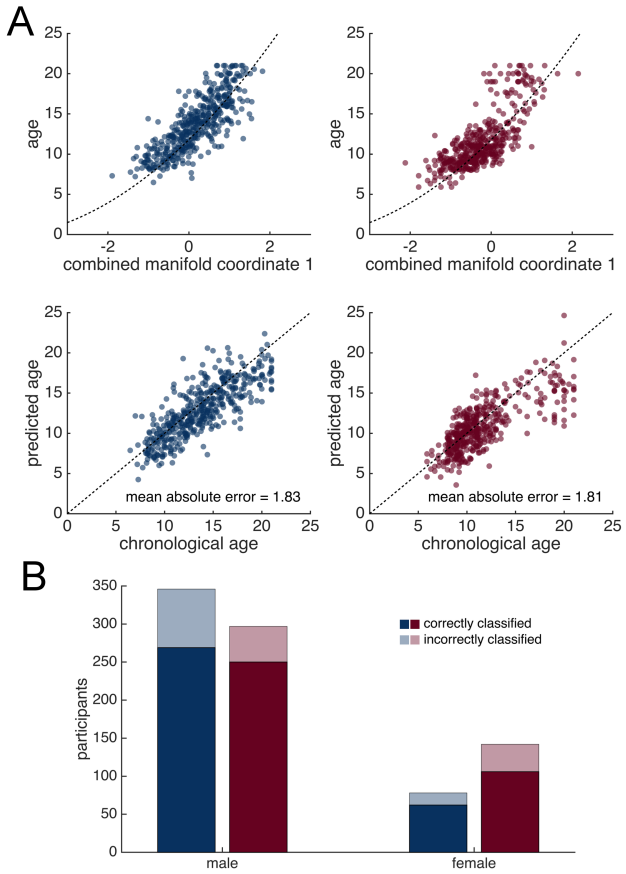

Figure 4: Age and sex prediction in typically-developing ABIDE and ABIDE-II participants. A. Scatterplots show ABIDE (blue) and ABIDE-II (red) data projected onto the manifold constructed from the full PING dataset. Line indicates a polynomial model fit on PING data. B. Correctly and incorrectly classified male and female participants in both groups are shown.

Associations with cognition

In order to determine if deviations from the average developmental trajectory of the brain coincided with cognitive performance we compared predicted age errors (the difference between age estimated from MRI using the above model and true, chronological age) with cognitive scores in PING and ABIDE.

In the PING cohort, no significant associations were found between NTCB scores (corrected for age, sex, socioeconomic status and genetic ancestry) and predicted age error after correcting for multiple comparisons (Table 2).

We repeated this analysis using predicted age estimates form 10-fold cross-validation in typically-developing participants from the ABIDE and ABIDE-II cohorts (n=802 with cognitive scores). Using full scale IQ as a measure of cognitive performance, we found no strong evidence for an association with predicted age error ($F_{1,800}$=3.82, p=0.051). This remained the case when after correcting FSIQ for effects of site and sex ($F_{1,800}$=3.089, p=0.079).

Table 2: Associations between predicted age error and cognitive score in PING

	Linear regression		
NTCB score	**R^2**	**$F_{1,615}$**	**p**
Flanker	0.001	0.35	0.556
Attention	0.001	0.619	0.432
Picture Sequence Memory	0.008	4.948	0.026
List Sorting	0.002	1.076	0.300
Picture Vocabulary	0.002	1.359	0.244
Reading	0.000	0.223	0.637
Dimensional Change Card Sorting	0.002	1.084	0.298
Pattern Comparison	0.008	5.055	0.025

Discussion

The brain follows a well-defined developmental trajectory during childhood, with tissue-specific alterations that reflect complex and ongoing biological processes including myelination and synaptic pruning. Accurate identification and modelling of these anatomical processes *in vivo* with MRI may provide clinically useful imaging markers of individual variability in development. In this study, we use manifold learning to generate a parsimonious description of typical brain development during childhood and adolescence. By combining measures of tissue volume, cortical thickness and cortical area, we show how patterns of anatomical variation can be used to accurately predict age and sex between the ages of 3 and 21 years. We show that this model is not strongly affected by site-to-site variation in image acquisition and yields accurate predictions across different study populations. In contrast to previous reports, however, we do not find strong evidence that deviation from a predicted trajectory corresponds to adverse functional or behavioural outcome in healthy individuals.

We demonstrate that biological age can be predicted from MRI in developmental populations with a mean error of around 1.6 years. This is in line with previous reports in this population. Using a set of 231 pre-selected, image-based features from T1, T2 and diffusion-weighted MRI, Brown et al. developed a nonlinear model of cerebral maturation to predict age in the PING cohort, achieving an MAE of 1.03 years (Brown et al. 2012). Using just T1-weighted image features, Brown et al. reported an MAE of 1.71y, comparable to the MAE reported in this study. Similarly, they also found that model accuracy decreased slightly with increasing age, suggesting that image-based prediction is most accurate during the periods when the rate of anatomical change is greatest (Dekaban 1978; Brown et al. 2012). Using a similar approach, Franke et al. reported an MAE of 1.1 years in a developmental cohort aged 5 to 18 (Franke et al. 2012). Using nonlinear mapping functions (i.e.: kernels) in machine learning allows for the use of linear methods to discover highly nonlinear boundaries or patterns in the original data by creating an implicit feature space (Hofmann et al. 2008). While flexible, a limitation of these methods is the inability to identify important features in the space of the original dataset. By calculating a linear mapping between the original, high-dimensional data and the low-dimensional embedded manifold, NPE produces a set of basis vectors that – through linear combination – can approximately reconstruct the original dataset, capture nonlinear relationships and provide interpretable maps of feature importance (He et al. 2005).

We show examples of these vectors in Figure 2 for each image metric. As reported previously, the anatomical patterns of variation associated with increasing age reflected a lower-to-higher-order trajectory characterised by reduced tissue volume and cortical thinning in frontal and parietal association cortex compared to primary sensory regions (Gogtay et al. 2004; Sowell et al. 2004). This was coupled with increased white matter tissue and brain stem volume (Xie et al. 2012; Aubert-Broche et al. 2013). Increasing age was also associated with increased cortical surface area most prominent in the insula and cingulate cortex. This agrees with previous reports of high rates of cortical surface area expansion during childhood in regions associated with higher-order intellectual function (Fjell et al. 2015; Amlien et al. 2016).

Sexual dimorphism during development is a contentious issue. Developmental trajectories for cortical grey and white matter appear similar between sexes (Aubert-Broche et al. 2013; Mills et al. 2016) with perceived sex differences often assigned to variation in physical size (Dekaban 1978; Giedd et al. 2012). However, even after accounting for total brain volume, regional volumetric differences and variations in the shape of tissue-specific developmental trajectories reported, with developmental 'peaks' in volume and cortical thickness observed at earlier timepoints in females than males (Lenroot et al. 2007; Koolschijn and Crone 2013). In a longitudinal study of 387 subjects aged 3 to 27, Lenroot et al. reported increased frontal grey matter volume in females and increased occipital white matter in males, after accounting for brain size (Lenroot et al. 2007). Conversely, Sowell et al. reported thicker parietal and posterior temporal cortex in females, independent of age (Sowell et al. 2007). These discrepant findings may reflect the different timing of puberty or the differential effects of testosterone on brain development males and females (Bramen et al. 2012).

Here, we find that female sex is predicted by a pattern of neuroanatomical variation comprising of reduced brain tissue volume in the posterior cingulate and precuneus, medial temporal lobe and occipital lobe, alongside a pattern of reduced cortical surface area across frontal and temporal regions and increased cortical thickness in the insula. We highlight that the manifold embedding coordinates defined by NPE are orthogonal by construction; as such, the patterns shown in Figure 2 reflect anatomical variation independently associated with age and sex during development. We do not anticipate that these patterns reflect global differences in head, or brain size between sexes. NPE aims

to optimally preserve the local neighbourhood structure embedded in the data (constrained in this case to be among similar aged participants, and within sex), therefore, given the relative stability of intracranial volume over this period, we did not expect our model to be driven by global volumetric changes due to head size (Lebel and Beaulieu 2011; Mills and Tamnes 2014). We confirmed this by showing that accounting for tissue volume change due to global scaling during image registration did not affect our results. Importantly, our study confirms recent reports that multivariate analyses that consider whole-brain patterns of variation in brain morphometry can reliably and accurately discriminate sex, even if large within-class, or between region, variability exists (Chekroud et al. 2016; Rosenblatt 2016). We also show that this dimorphic pattern is evident even at very young ages, achieving a classification accuracy of around 69% in the youngest participants (aged 3-5y). It is important to consider that this finding does not imply that all females have a smaller posterior cingulate than all males, or even that the cingulate is on average smaller in females across populations. We suggest that this pattern of variation is one of a number (including the pattern of age-related variation described above) that exist concurrently within a population. An individual's anatomical phenotype can then be viewed as arising from the weighted expression of these patterns, with the weight dependent on e.g.: age, sex, environmental or genetic factors. As such, tissue volume or cortical thickness, measured at a single point reflects the combination of multiple, distributed patterns of variation and, as such, may vary greatly over a population and not necessarily in line with a given covariate of interest (e.g.: sex).

Surprisingly, and in contrast to previous reports, we do not find strong evidence that a divergent image-based age prediction is a good marker of cognitive function. Using a multi-modal approach, that also included measures derived from diffusion MRI, the discrepancy between chronological age and an image-based estimate of 'brain age' has been proposed as a possible biomarker of cognitive development (Erus et al. 2015). This follows on from studies in older populations, where a more advanced 'brain age' was used as a marker of aging and found to correlate with brain injury (Cole et al. 2015) and dementia (Gaser et al. 2013). In this study, we tested this hypothesis in two large, independent, developmental cohorts. Using cross-validated age predictions, we did not find any statistically significant associations between measures of cognitive function (NCTB scores in PING; FSIQ in ABIDE) and age prediction error in typically-developing individuals. In the PING cohort, Akshoomoff et al., found that age, sex, socioeconomic status and genetic ancestry explained between 57% and 73% of variance in each of the NCTB scores (Akshoomoff et al. 2014). After correcting for these factors, we found that brain age estimation error explained at most 0.8% of the remaining variance (in memory and pattern comparison tests). In the ABIDE cohort, FSIQ showed a weak association with age estimation error, although this failed to reach statistical significance. This suggests that model error in age prediction does not reflect the impact of an underlying latent variable associated with cognition. This discrepancy is likely due to differences in model construction between methods. Here, we use NPE to extract a single dimension of anatomical variation that aims to maximally preserve specific age-related structure in the data. As such, the reported pattern may lie orthogonal to neuroanatomical correlates of (non age-related) cognitive performance and as mentioned above, such patterns, while coexistent within the population, may not vary as a function of each other. Other methods that predict age based on how the appearance of the brain as a whole, might better reflect the conflation of cognitive and age-related 'components' during development, such that model error captures variation in anatomy aligned with cognition (Erus et al. 2015).

Our findings suggest that the anatomical maturation of the brain during childhood and adolescence can be accurately modeled within a low-dimensional subspace. That is, variation along two axes is sufficient to capture individual variations due to age and sex within a population with high accuracy. In contrast, functional or cognitive development is not well represented by variation along these axes. This suggests that additional, orthogonal dimensions of development are required to more accurately model individual trajectories. Alternatively, this approach may benefit from incorporating information from additional imaging modalities (e.g.: functional MRI) in order to more fully capture phenotypic variation associated with cognitive development (Erus et al. 2015; Liem et al. 2017). Indeed, combining functional, diffusion and possibly genetic information into a larger manifold framework and considering similarities over multiple modalities to model local neighbourhoods and communities within large datasets could provide a more complete model of individual variation during this time period. In addition, the projection of longitudinal data onto the manifold could enable individuals to be tracked over time, an important consideration for developmental studies (Mills and Tamnes 2014).

In summary, we present a framework for modelling anatomical development during childhood. This model accurately predicts age and sex based on image-derived markers of cerebral morphology and generalises well to independent populations.

Acknowledgements

This research was conducted within the Developmental Imaging research group, Murdoch Childrens Research Institute and the Children's MRI Centre, Royal Children's Hospital, Melbourne, Victoria. It was supported by the Murdoch Childrens Research Institute, the Royal Children's Hospital, Department of Paediatrics, The University of Melbourne and the Victorian Government's Operational Infrastructure Support Program. The project was generously supported by RCH1000, a unique arm of The Royal Children's Hospital Foundation devoted to raising funds for research at The Royal Children's Hospital.

Data collection and sharing for this project was funded by the Pediatric Imaging, Neurocognition and Genetics Study (PING) (NIH: RC2DA029475). PING is funded by the National Institute on Drug Abuse and the Eunice Kennedy Shriver National Institute of Child Health & Human Development. PING data are disseminated by the PING Coordinating Center at the Center for Human Development, University of California, San Diego.

The authors would also like to thank Adriana Di Martino, Michael P Milham and all involved in the collection and aggregation of the ABIDE and ABIDE-II datasets.

References

Akshoomoff N, Newman E, Thompson WK, McCabe C, Bloss CS, Chang L, Amaral DG, Casey BJ, Ernst TM, Frazier JA, Gruen JR, Kaufmann WE, Kenet T, Kennedy DN, Libiger O, Mostofsky S, Murray SS, Sowell ER, Schork N, Dale AM, Jernigan TL. 2014. The NIH Toolbox Cognition Battery: Results from a Large Normative Developmental Sample (PING). Neuropsychology. 28:1–10.

Aljabar P, Wolz R, Srinivasan L, Counsell S, Rutherford M, Edwards A, Hajnal J, Rueckert D. 2011. A combined manifold learning analysis of shape and appearance to characterize neonatal brain development. IEEE Trans Med Imaging. 30:2072–2086.

Amlien IK, Fjell AM, Tamnes CK, Grydeland H, Krogsrud SK, Chaplin TA, Rosa MGP, Walhovd KB. 2016. Organizing Principles of Human Cortical Development—Thickness and Area from 4 to 30 Years: Insights from Comparative Primate Neuroanatomy. Cereb Cortex. 26:257–267.

Ashburner J, Hutton C, Frackowiak R, Johnsrude I, Price C, Friston K. 1998. Identifying global anatomical differences: deformation-based morphometry. Hum Brain Mapp. 6:348–357.

Aubert-Broche B, Fonov VS, García-Lorenzo D, Mouiha A, Guizard N, Coupé P, Eskildsen SF, Collins DL. 2013. A new method for structural volume analysis of longitudinal brain MRI data and its application in studying the growth trajectories of anatomical brain structures in childhood. NeuroImage. 82:393–402.

Avants BB, Epstein CL, Grossman M, Gee JC. 2008. Symmetric diffeomorphic image registration with cross-correlation: evaluating automated labeling of elderly and neurodegenerative brain. Med Image Anal. 12:26–41.

Bramen JE, Hranilovich JA, Dahl RE, Chen J, Rosso C, Forbes EE, Dinov ID, Worthman CM, Sowell ER. 2012. Sex Matters during Adolescence: Testosterone-Related Cortical Thickness Maturation Differs between Boys and Girls. PLoS ONE. 7:e33850.

Brown TT, Kuperman JM, Chung Y, Erhart M, McCabe C, Hagler DJ, Venkatraman VK, Akshoomoff N, Amaral DG, Bloss CS, Casey BJ, Chang L, Ernst TM, Frazier JA, Gruen JR, Kaufmann WE, Kenet T, Kennedy DN, Murray SS, Sowell ER, Jernigan TL, Dale AM. 2012. Neuroanatomical assessment of biological maturity. Curr Biol CB. 22:1693–1698.

Chekroud AM, Ward EJ, Rosenberg MD, Holmes AJ. 2016. Patterns in the human brain mosaic discriminate males from females. Proc Natl Acad Sci U S A. 113:E1968.

Cole JH, Leech R, Sharp DJ, Alzheimer's Disease Neuroimaging Initiative. 2015. Prediction of brain age suggests accelerated atrophy after traumatic brain injury. Ann Neurol. 77:571–581.

Dale AM, Fischl B, Sereno MI. 1999. Cortical Surface-Based Analysis: I. Segmentation and Surface Reconstruction. NeuroImage. 9:179–194.

Dekaban AS. 1978. Changes in brain weights during the span of human life: relation of brain weights to body heights and body weights. Ann Neurol. 4:345–356.

Di Martino A, O'Connor D, Chen B, Alaerts K, Anderson JS, Assaf M, Balsters JH, Baxter L, Beggiato A, Bernaerts S, Blanken LME, Bookheimer SY, Braden BB, Byrge L, Castellanos FX, Dapretto M, Delorme R, Fair DA, Fishman I, Fitzgerald J, Gallagher L, Keehn RJJ, Kennedy DP, Lainhart JE, Luna B, Mostofsky SH, Müller R-A, Nebel MB, Nigg JT, O'Hearn K, Solomon M, Toro R, Vaidya CJ, Wenderoth N, White T, Craddock RC, Lord C, Leventhal B, Milham MP. 2017. Enhancing studies of the connectome in autism using the autism brain imaging data exchange II. Sci Data. 4:170010.

Di Martino A, Yan C-G, Li Q, Denio E, Castellanos FX, Alaerts K, Anderson JS, Assaf M, Bookheimer SY, Dapretto M, Deen B, Delmonte S, Dinstein I, Ertl-Wagner B, Fair DA, Gallagher L, Kennedy DP, Keown CL, Keysers C, Lainhart JE, Lord C, Luna B, Menon V, Minshew NJ, Monk CS, Mueller S, Müller R-A, Nebel MB, Nigg JT, O'Hearn K, Pelphrey KA, Peltier SJ, Rudie JD, Sunaert S, Thioux M, Tyszka JM, Uddin LQ, Verhoeven JS, Wenderoth N, Wiggins JL, Mostofsky SH, Milham MP. 2014. The autism brain imaging data exchange: towards a large-scale evaluation of the intrinsic brain architecture in autism. Mol Psychiatry. 19:659–667.

Dosenbach NUF, Nardos B, Cohen AL, Fair DA, Power JD, Church JA, Nelson SM, Wig GS, Vogel AC, Lessov-Schlaggar CN, Barnes KA, Dubis JW, Feczko E, Coalson RS, Pruett JR, Barch DM, Petersen SE, Schlaggar BL. 2010. Prediction of Individual Brain Maturity Using fMRI. Science. 329:1358–1361.

Erus G, Battapady H, Satterthwaite TD, Hakonarson H, Gur RE, Davatzikos C, Gur RC. 2015. Imaging Patterns of Brain Development and their Relationship to Cognition. Cereb Cortex. 25:1676–1684.

Fischl B, Dale AM. 2000. Measuring the thickness of the human cerebral cortex from magnetic resonance images. Proc Natl Acad Sci U S A. 97:11050–11055.

Fischl B, Salat DH, Busa E, Albert M, Dieterich M, Haselgrove C, van der Kouwe A, Killiany R, Kennedy D, Klaveness S, Montillo A, Makris N, Rosen B, Dale AM. 2002. Whole brain segmentation: automated labeling of neuroanatomical structures in the human brain. Neuron. 33:341–355.

Fischl B, Sereno MI, Dale AM. 1999. Cortical Surface-Based Analysis: II: Inflation, Flattening, and a Surface-Based Coordinate System. NeuroImage. 9:195–207.

Fjell AM, Westlye LT, Amlien I, Tamnes CK, Grydeland H, Engvig A, Espeseth T, Reinvang I, Lundervold AJ, Lundervold A, Walhovd KB. 2015. High-Expanding Cortical Regions in Human Development and Evolution Are Related to Higher Intellectual Abilities. Cereb Cortex. 25:26–34.

Franke K, Luders E, May A, Wilke M, Gaser C. 2012. Brain maturation: predicting individual BrainAGE in children and adolescents using structural MRI. NeuroImage. 63:1305–1312.

Franke K, Ziegler G, Klöppel S, Gaser C. 2010. Estimating the age of healthy subjects from T1-weighted MRI scans using kernel methods: Exploring the influence of various parameters. NeuroImage. 50:883–892.

Gaser C, Franke K, Klöppel S, Koutsouleris N, Sauer H, Alzheimer's Disease Neuroimaging Initiative. 2013. BrainAGE in Mild Cognitive Impaired Patients: Predicting the Conversion to Alzheimer's Disease. PloS One. 8:e67346.

Giedd JN, Blumenthal J, Jeffries NO, Castellanos FX, Liu H, Zijdenbos A, Paus T, Evans AC, Rapoport JL. 1999. Brain development during childhood and adolescence: a longitudinal MRI study. Nat Neurosci. 2:861–863.

Giedd JN, Raznahan A, Mills KL, Lenroot RK. 2012. Review: magnetic resonance imaging of male/female differences in human adolescent brain anatomy. Biol Sex Differ. 3:19.

Giedd JN, Stockman M, Weddle C, Liverpool M, Alexander-Bloch A, Wallace GL, Lee NR, Lalonde F, Lenroot RK. 2010. Anatomic Magnetic Resonance Imaging of the Developing Child and Adolescent Brain and Effects of Genetic Variation. Neuropsychol Rev. 20:349–361.

Gogtay N, Giedd JN, Lusk L, Hayashi KM, Greenstein D, Vaituzis AC, Nugent TF, Herman DH, Clasen LS, Toga AW, Rapoport JL, Thompson PM. 2004. Dynamic mapping of human cortical development during childhood through early adulthood. Proc Natl Acad Sci U S A. 101:8174–8179.

He X, Cai D, Yan S, Zhang H-J. 2005. Neighborhood preserving embedding. In: Tenth IEEE International Conference on Computer Vision (ICCV'05) Volume 1. p. 1208–1213 Vol. 2.

Hofmann T, Schölkopf B, Smola AJ. 2008. Kernel Methods in Machine Learning. Ann Stat. 36:1171–1220.

Huttenlocher PR. 1979. Synaptic density in human frontal cortex - developmental changes and effects of aging. Brain Res. 163:195–205.

Jernigan TL, Brown TT, Hagler Jr. DJ, Akshoomoff N, Bartsch H, Newman E, Thompson WK, Bloss CS, Murray SS, Schork N, Kennedy DN, Kuperman JM, McCabe C, Chung Y, Libiger O, Maddox M, Casey BJ, Chang L, Ernst TM, Frazier JA, Gruen JR, Sowell ER, Kenet T, Kaufmann WE, Mostofsky S, Amaral DG, Dale AM. 2016. The Pediatric Imaging, Neurocognition, and Genetics (PING) Data Repository. NeuroImage, Sharing the wealth: Brain Imaging Repositories in 2015. 124, Part B:1149–1154.

Koolschijn PCMP, Crone EA. 2013. Sex differences and structural brain maturation from childhood to early adulthood. Dev Cogn Neurosci. 5:106–118.

Lebel C, Beaulieu C. 2011. Longitudinal Development of Human Brain Wiring Continues from Childhood into Adulthood. J Neurosci. 31:10937–10947.

Lenroot RK, Giedd JN. 2008. The changing impact of genes and environment on brain development during childhood and adolescence: Initial findings from a neuroimaging study of pediatric twins. Dev Psychopathol. 20:1161–1175.

Lenroot RK, Gogtay N, Greenstein DK, Wells EM, Wallace GL, Clasen LS, Blumenthal JD, Lerch J, Zijdenbos AP, Evans AC, Thompson PM, Giedd JN. 2007. Sexual dimorphism of brain developmental trajectories during childhood and adolescence. NeuroImage. 36:1065–1073.

Libiger O, Schork NJ. 2012. A Method for Inferring an Individual's Genetic Ancestry and Degree of Admixture Associated with Six Major Continental Populations. Front Genet. 3:322.

Liem F, Varoquaux G, Kynast J, Beyer F, Kharabian Masouleh S, Huntenburg JM, Lampe L, Rahim M, Abraham A, Craddock RC, Riedel-Heller S, Luck T, Loeffler M, Schroeter ML, Witte AV, Villringer A, Margulies DS. 2017. Predicting brain-age from multimodal imaging data captures cognitive impairment. NeuroImage. 148:179–188.

Löwe LC, Gaser C, Franke K, Alzheimer's Disease Neuroimaging Initiative. 2016. The Effect of the APOE Genotype on Individual BrainAGE in Normal Aging, Mild Cognitive Impairment, and Alzheimer's Disease. PloS One. 11:e0157514.

Mills KL, Goddings A-L, Herting MM, Meuwese R, Blakemore S-J, Crone EA, Dahl RE, Güroğlu B, Raznahan A, Sowell ER, Tamnes CK. 2016. Structural brain development between childhood and adulthood: Convergence across four longitudinal samples. NeuroImage. 141:273–281.

Mills KL, Tamnes CK. 2014. Methods and considerations for longitudinal structural brain imaging analysis across development. Dev Cogn Neurosci. 9:172–190.

Minka TP. 2001. Automatic Choice of Dimensionality for PCA. In: Leen TK,, Dietterich TG,, Tresp V, editors. Advances in Neural Information Processing Systems 13. MIT Press. p. 598–604.

Raznahan A, Shaw P, Lalonde F, Stockman M, Wallace GL, Greenstein D, Clasen L, Gogtay N, Giedd JN. 2011. How Does Your Cortex Grow? J Neurosci. 31:7174–7177.

Richmond S, Johnson KA, Seal ML, Allen NB, Whittle S. 2016. Development of brain networks and relevance of environmental and genetic factors: A systematic review. Neurosci Biobehav Rev. 71:215–239.

Rosenblatt JD. 2016. Multivariate revisit to "sex beyond the genitalia." Proc Natl Acad Sci U S A. 113:E1966–E1967.

Roweis ST, Saul LK. 2000. Nonlinear dimensionality reduction by locally linear embedding. Science. 290:2323–2326.

Rueckert D, Frangi AF, Schnabel JA. 2003. Automatic construction of 3-D statistical deformation models of the brain using nonrigid registration. Med Imaging IEEE Trans On. 22:1014–1025.

Sowell ER, Peterson BS, Kan E, Woods RP, Yoshii J, Bansal R, Xu D, Zhu H, Thompson PM, Toga AW. 2007. Sex differences in cortical thickness mapped in 176 healthy individuals between 7 and 87 years of age. Cereb Cortex N Y N 1991. 17:1550–1560.

Sowell ER, Thompson PM, Leonard CM, Welcome SE, Kan E, Toga AW. 2004. Longitudinal Mapping of Cortical Thickness and Brain Growth in Normal Children. J Neurosci. 24:8223–8231.

Tamnes CK, Walhovd KB, Dale AM, Østby Y, Grydeland H, Richardson G, Westlye LT, Roddey JC, Hagler Jr. DJ, Due-Tønnessen P, Holland D, Fjell AM. 2013. Brain development and aging: Overlapping and unique patterns of change. NeuroImage. 68:63–74.

Tustison NJ, Avants BB, Cook PA, Zheng Y, Egan A, Yushkevich PA, Gee JC. 2010. N4ITK: Improved N3 Bias Correction. IEEE Trans Med Imaging. 29:1310–1320.

Wierenga LM, Langen M, Oranje B, Durston S. 2014. Unique developmental trajectories of cortical thickness and surface area. NeuroImage. 87:120–126.

Xie Y, Chen YA, De Bellis MD. 2012. The relationship of age, gender, and IQ with the brainstem and thalamus in healthy children and adolescents: a magnetic resonance imaging volumetric study. J Child Neurol. 27:325–331.

Yakovlev PI, Lecours AR. 1967. The myelogenetic cycles of regional maturation of the brain. In: Regional Development of the Brain in Early Life. Oxford: Blackwell. p. 3–69.

Zeng X, Luo S. 2007. A Supervised Subspace Learning Algorithm: Supervised Neighborhood Preserving Embedding. In: Alhajj R,, Gao H,, Li J,, Li X,, Zaïane OR, editors. Advanced Data Mining and Applications. Lecture Notes in Computer Science. Presented at the International Conference on Advanced Data Mining and Applications. Springer Berlin Heidelberg. p. 81–88.

Supplemental Materials

Table S1: PING demographics by site

Site	n	age (range)	Male
a	112	15.14 (4.08-21.0)	57 (50.8)
b	105	14.69 (3.75-21.0)	59 (56.2)
c	118	12.29 (3.17-21.0	58 (49.2)
d	124	12.03 (3.17-20.92)	68 (54.8)
e	64	13.42 (4.17-20.92)	34 (53.1)
f	129	8.79 (3.25-20.25)	65 (50.4)
g	116	10.87 (3.42-21.00)	63 (54.3)
Total	768	12.28 (3.17-21.0)	404 (52.6)

Table S2: ABIDE and ABIDE-II demographics by site

	ABIDE		
Site	**n**	**age (range)**	**male (%)**
a	19	15.30 (9.44-20.65)	16 (84.2)
b	15	16.53 (10.0-21.0)	13 (86.7)
c	15	10.06 (8.20-11.99)	15 (100)
d	22	14.22 (8.67-16.88)	16 (72.8)
e	21	16.28 (12.04-20.33)	21 (100)
f	72	14.48 (8.2-19.2)	54 (75.0)
g	22	15.31 (8.77-19.76)	22 (100)
h	28	12.68 (7.66-17.83)	20 (71.4)
i	4	20.75 (20.0-21.0)	3 (75.0)
j	23	15.08 (12.20-21.0)	18 (78.2)
k	24	10.01 (8.07-12.77)	20 (83.3)
l	82	13.08 (6.47-20.56)	63 (76.8)
m	20	9.95 (7.75-12.43)	16 (80.0)
n	43	12.96 (9.21-17.79)	37 (86.0)
o	7	12.57 (7.00-21.00)	7 (100)
p	6	19.52 (17.0-20.90)	4 (66.7)
q	1	20 (-)	1 (-)
Total	424	13.69 (6.47-21.0)	346 (81.6)

	ABIDE-II		
Site	**n**	**age (range)**	**male (%)**
a	10	19.6 (18.0-21.0)	7 (80.0)
b	52	10.45 (8.06-13.80)	26 (50.0)
c	25	13.25 (8.10-17.70)	23 (92.0)
d	56	10.38 (8.0-14.0)	27 (48.2)
e	7	19.43 (18.0-21.0)	7 (100)
f	6	17.89 (13.83-20.17)	6 (100)
g	21	15.61 (10.25-20.0)	21 (100)
h	28	9.06 (5.89-12.9)	27 (96.4)
i	154	10.35 (8.02-12.90)	99 (64.2)
j	5	14.79 (11.50-18.58)	5 (100)
k	8	20.25 (19.0-21.0)	6 (75.0)
l	12	14.30 (8.17-20.51)	3 (25.0)
m	15	9.81 (7.76-14.09)	10 (66.7)
n	25	8.15 (6.33-10.12)	20 (80.0)
o	14	14.80 (12.25-17.17)	10 (71.4)
Total	438	11.5 (5.89-21.00)	297 (67.7)